ISSN 1067-8212, Russian Journal of Non-Ferrous Metals, 2022, Vol. 63, No. 4, pp. 434–440. © Allerton Press, Inc., 2022.
Russian Text © The Author(s), 2022, published in Izvestiya Vysshikh Uchebnykh Zavedenii, Tsvetnaya Metallurgiya, 2022, No. 3, pp. 77–85.

PHYSICAL METALLURGY AND HEAT TREATMENT

Structure and Properties of Al–Cu–Yb Alloy with Iron and Silicon Impurities

M. V. Barkov[a], *, O. I. Mamzurina[a], **, M. V. Glavatskikh[a], *, R. Yu. Barkov[a], ****, and A. V. Pozdniakov[a], *******

[a] *National University of Science and Technology (NUST) MISiS, Moscow, 119991 Russia*

**e-mail: erconu@yandex.ru*

***e-mail: mamzurina.oi@misis.ru*

****e-mail: glavatskikh@edu.misis.ru*

*****e-mail: barkov@misis.ru*

******e-mail: pozdniakov@misis.ru*

Received February 25, 2022; revised March 23, 2022; accepted March 25, 2022

Abstract—The effect of iron and silicon impurities on the phase composition and properties of the Al–4.3Cu–2.2Yb quasi-binary alloy has been determined. In the microstructure of the cast alloy, in addition to the aluminum solid solution and dispersed eutectic ((Al) + Al_8Cu_4Yb), in which about 1% of iron is dissolved, the $Al_3Yb/(Al,Cu)_{17}Yb_2$ and $Al_{80}Yb_5Cu_6Si_8$ phases are identified, which are not found in an alloy of a similar composition without impurities. After homogenization annealing at a temperature of 590°C for 3 h, the structure is represented by compact fragmented and coagulated intermetallic compounds 1–2 μm in size and a solid solution (Al) with a maximum copper content of 2.1%. The hardness of the deformed sheets significantly decreases after 0.5 h and changes slightly up to 6 h of annealing at temperatures of 150–210°C. After annealing at 180°C for 3 h, a substructure with a subgrain size of 200–400 nm is formed in the alloy structure. The softening after annealing of the rolled sheets at temperatures up to 250°C occurs owing to the recovery and polygonization processes and above 300°C owing to recrystallization. After annealing for 1 h at 300°C, the recrystallized grain size is 7 μm. The grain size increases to 16 μm after annealing for 1 h at 550°C. The Al–4.3Cu–2.2Yb alloy with impurities has a conditional yield strength of 205–273 MPa, a tensile strength of 215–302 MPa, and a relative elongation of 2.3–5.6% in the rolled alloy after annealing. Iron and silicon impurities do not lead to the formation of coarse lamellar intermetallic phases and do not reduce the ductility of the investigated alloy.

Keywords: aluminum alloys, ytterbium, impurities, microstructure, phase composition, hardness

DOI: 10.3103/S1067821222040034

INTRODUCTION

The effect of iron and silicon impurities on the phase composition of aluminum alloys, their microstructure, and their properties must be estimated in the development of new materials. Depending on the content of impurities and their ratio in Al alloys, the phase morphology can change significantly, affecting both the final mechanical characteristics and technological effectiveness under pressure processing [1, 2].

It is necessary to study the effect of impurities during the production of new alloys. The alloys doped with rare earth metals (REM) have been extensively developed in recent years. Small additives of REM are only used for alloying, but they are applied as the main doping components for cast and wrought alloys. The alloys of quasi-binary sections of ternary systems Al–Ce–Cu [3, 4], Al–Cu–Y [5–10], Al–Cu–Er [6, 9–14], Al–Cu–Yb, and Al–Cu–Gd [15] are shown to be promising for the development of new high-tech and heat-resistant cast and wrought alloys [9, 10]. Alloys in ternary systems have a narrow crystallization range; eutectic phases have a high resistance to coagulation [3–6, 11, 15]. Alloying with zirconium, manganese, titanium, and especially magnesium significantly improves the strength characteristics of alloys [7–10, 12–14]. The presence of 0.15% iron and silicon impurities in Al–Cu–Y, Al–Cu–Er, and Al–Cu–Gd ternary alloys results in the crystallization of silicon-containing phases $Al_{11}Cu_2Y_2Si_2$, $Al_3Er_2Si_2$, and $Al_{80}Gd_5Cu_8Si_5$, respectively [16–18]. Iron dissolves in other crystalline phases without the formation of coarse lamellar phases. In dilute alloys, silicon causes the acceleration of dispersion strengthening during the annealing of ingots in the presence of REM [19–21]. In an Al–Y–Sc alloy containing iron and silicon impurities, the AlYFeSi phase is formed during crystallization, and scandium is completely dissolved in

the aluminum solid solution [22]. The reinforcement of the Al–Y–Er–Zr–Sc alloy is reduced because of the particular binding of zirconium, erbium, and yttrium into the crystalline phases containing iron and silicon AlSiFeEr(Zr)) and (AlSiErY(Zr) [23]. Alloys doped with ytterbium together with other REM demonstrate good properties owing to the dispersoids formed during ingot annealing [24–34]. Small additives of ytterbium in aluminum alloys increase corrosion resistance [31, 32] and can be an adequate replacement for expensive scandium in magnaliums.

Quasi-binary alloys with a large amount of the eutectic phase are an alternative for alloying with eutectic-forming elements in the development of new cast aluminum alloys [35–42]. In particular, the Al–Cu–Yb alloy [15] having a Cu/Yb atomic ratio of 4/1 is located in a quasi-binary section [43] and is characterized by a narrow crystallization range and good mechanical properties owing to the presence of the Al_8Cu_4Yb and Al_3Yb phases. To expand the field of application of these alloys, the effect of iron and silicon impurities on their properties should be studied.

The work studies the structure and properties of rolled ternary quasi-binary alloy Al–4.3Cu–2.2Yb containing 0.3% Fe and Si impurities.

EXPERIMENTAL

The alloy was melted in a resistance furnace using aluminum (99.7%), copper (99.9%), and Al–10Yb master alloy. The melt was poured into a water-cooled copper mold with an internal cavity of 20 × 40 × 100 mm at a heating rate of 15 K/s. Heat treatment was carried out in furnaces with fan control produced by Nabertherm (Germany) and AB UMEGA (Lithuania). The accuracy of maintaining the temperature in the furnaces was 1°C.

Cross sections were prepared using a Labopol-5 (Struers, Denmark) grinding and polishing system. Microstructural study and phase identification were conducted using a Zeiss (Germany) light microscope (LM) and a Vega 3LMH (Tescan, Czech Republic) scanning electron microscope (SEM) equipped with an X-Max 80 (Oxford Instruments, United Kingdom) energy-dispersive detector. Calorimetric analysis was performed using a differential scanning calorimeter (DSC) produced by Labsys Setaram (France). The X-ray diffraction study was conducted using a D8 Advance (Brucker, USA) diffractometer.

After heat treatment (homogenization at 590°C for 3 h), the ingot was rolled to a thickness of 10 mm at 440°C and a thickness of 1 mm at room temperature. Then, annealing was carried out at t = 100–550°C for various times. The hardness was measured by the Vickers method. Tensile tests were conducted using an AllroundLine Z250 (Zwick Roell AG, Germany) machine with an automatic longitudinal strain sensor.

RESULTS AND DISCUSSION

Figure 1a presents the microstructure of an ingot of the studied alloy which consists of aluminum solid solution (Al), dispersed eutectic, and individual light and gray inclusions. According to EDX results, the Cu content in (Al) is 1.6%, and the concentration of ytterbium and silicon does not exceed 0.2% for each element. The disperse eutectic contains Al and a phase enriched in Cu and Yb that also contains Fe (up to 1%) and Si (up to 0.7%). Areas with an increased concentration of silicon and iron corresponding to sections of the structure with separate light inclusions are depicted on element distribution maps (Fig. 1a). Gray particles (upper left corner of the distribution maps) are enriched only in copper.

According to the DSC results, the alloy solidus temperature is 602°C. Therefore, the ingot was homogenized at 590°C for 3 h. The homogenization mode is similar to that for an alloy of close composition without impurities [15].

Dissolution of a nonequilibrium excess of crystalline phases, fragmentation, and spheroidization of equilibrium intermetallic compounds occur during homogenization. After annealing for 3 h (Fig. 1b), the microstructure stabilizes; the particle size of excess phases is 1–2 μm, and the copper content in the solid solution reaches a maximum of 2.1%. Individual particles enriched in Cu, Yb, and Si with a size of 1.0–1.5 μm are formed in the microstructure during homogenization. EDX analysis demonstrates the presence of 20–30% Yb, 10–15% Cu, and 5–6% Si, which corresponds to the $Al_{80}Yb_6Cu_6Si_8$ phase when converted to atomic fractions. With regard to the features of the EDX analysis, the content of the main elements in the phase is underestimated because the analysis covers the matrix (Al) surrounding the particle. This fact has a negligible influence on a certain Yb/Cu/Si ratio in the $Al_{80}Yb_6Cu_6Si_8$ phase.

As for the alloy without impurities, Al_8Cu_4Yb is the main eutectic phase [15]. However, iron is dissolved in the particles of this phase without significant changes in the crystalline lattice parameters. The main peaks of this phase are revealed at θ = 32°–32.5°, 35.5°, 40°–41°, and 46° (XRD pattern of AlCuYbFeSi alloy). The same peaks are depicted in the XRD pattern of AlCuYb alloy without impurities (Fig. 2). Lighter inclusions in the microstructure can be attributed to the $Al_3Yb/(Al,Cu)_{17}Yb_2$ phase by the peak at θ = 37°. The peaks at θ = 31°, 33.5°, 37°, 46°, and 47.5°, which are absent in the XRD pattern of pure alloy, presumably are attributed to a phase with silicon admixture (AlYbCuSi) identified as $Al_{80}Yb_6Cu_6Si_8$. The $Al_{80}Gd_5Cu_8Si_5$ phase of close composition is found in the Al–Cu–Gd–Fe–Si alloy, and unidentified peaks are present in the XRD pattern of this alloy at similar angles [18].

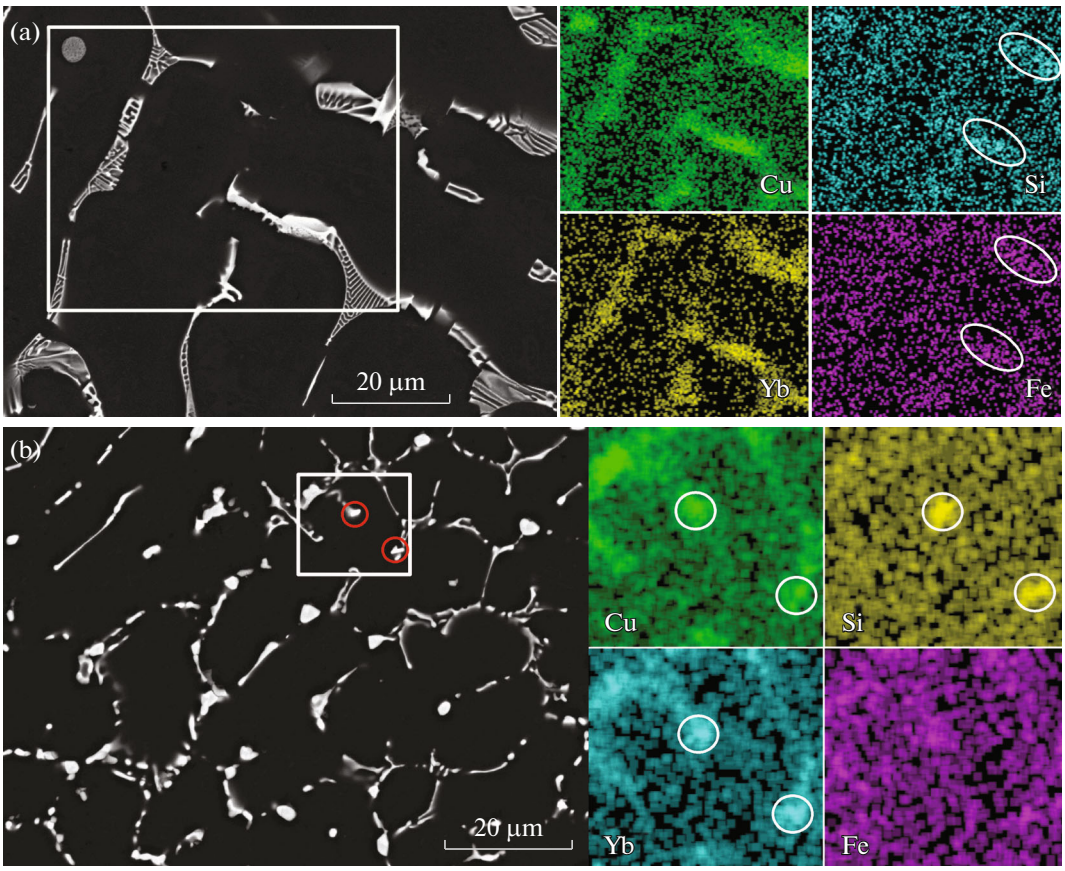

Fig. 1. Microstructure of as-cast alloy (a) and alloy after homogenization at 590°C for 3 h (b). The distribution of alloying elements between phases in the framed sections is shown.

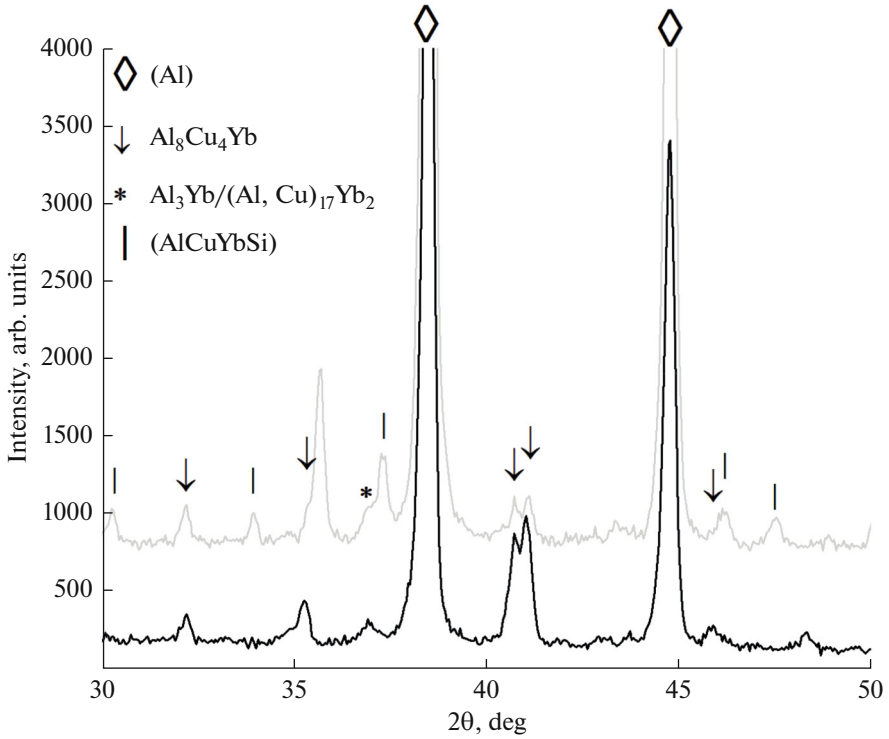

Fig. 2. XRD patterns of the studied AlCuYbFeSi alloy (gray line) and pure AlCuYb alloy (black line [15]).

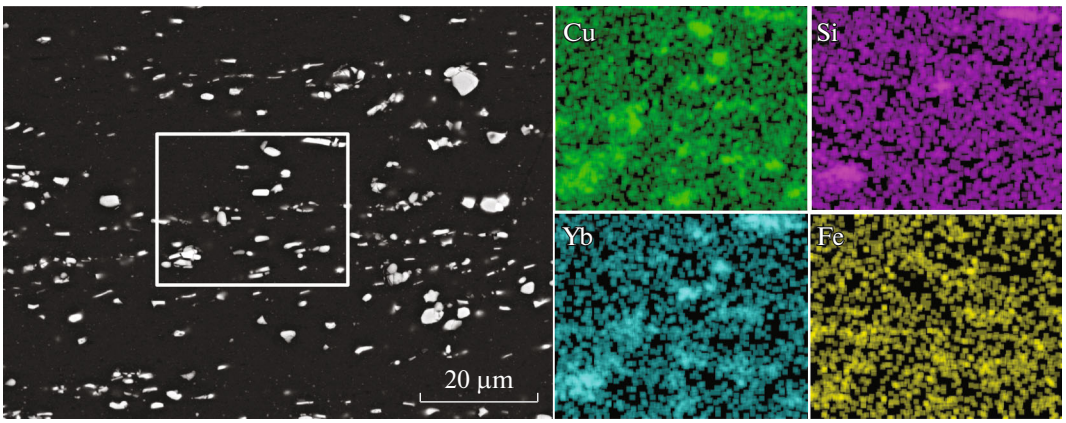

Fig. 3. Microstructure in cold-wrought state and distribution of alloying elements between phases in the framed section.

After homogenization at 590°C for 3 h, the alloy ingot was rolled into a sheet with a thickness of 1 mm. It is seen in Fig. 3 that excess phases are uniformly distributed in the microstructure during rolling, lining up toward deformation.

Figure 4 presents the dependences of hardness on annealing time at temperatures 150, 180, and 210°C and on annealing temperature for 1 h. After rolling, the hardness value is 101 ± 2 HV. During annealing at temperatures below 250°C, softening occurs owing to the processes of recovery and polygonization. The hardness decreases significantly after 0.5 h of annealing and then changes insignificantly up to $\tau = 6$ h at $t =$ 150–210°C (Fig. 4a).

As is seen in the inset in Fig. 4a, a substructure is formed in the alloy structure after annealing at 180°C for 3 h; the subgrain size is 200–400 nm. After annealing at temperatures up to 250°C, the grain structure in the alloy remains non-recrystallized (insets of structures in Fig. 4b). The recrystallization completely vanishes after annealing at 300°C for 1 h; the grain size is 7 μm (inset of microstructure in Fig. 4b). With increase in the annealing temperature of the deformed sheet to 550°C, the size of the recrystallized grain increases to 16 μm. The hardness of the alloy with impurities is higher than that of the pure alloy with close composition [15]. A similar effect of Fe and Si impurities on the properties was observed for Al–Cu–Y [16] and Al–Cu–Er [17] alloys.

Table 1 shows the values of the conditional yield strength ($\sigma_{0.2}$), ultimate tensile strength (σ_u), and elongation at fracture (δ) after uniaxial tensile tests in deformed and annealed states. The studied alloy demonstrates a high level of mechanical properties. The results on the yield strength are in good agreement with the hardness (Fig. 4). The yield strength in the deformed state is 290 MPa at the elongation of 2%. As the annealing temperature is increased from 100 to 180°C, the yield strength decreases from 273 to 227 MPa, and the relative elongation grows from 3.6 to 5.6%. The relative elongation of pure alloy remains the same: 3.1–5.6% [15].

Table 1. Characteristics of mechanical properties of the studied alloy after uniaxial tensile tests in deformed and annealed states

Annealing temperature for 1 h, °C	$\sigma_{0.2}$, MPa	σ_u, MPa	δ, %
No annealing (pure alloy)	303 ± 2	327 ± 2	3.2 ± 0.8
No annealing	290 ± 5	320 ± 6	2.0 ± 0.2
100	273 ± 2	302 ± 4	3.6 ± 0.4
150	238 ± 1	262 ± 1	4.2 ± 0.4
180	227 ± 1	243 ± 3	5.6 ± 0.8
210	205 ± 5	215 ± 3	4.0 ± 2.0

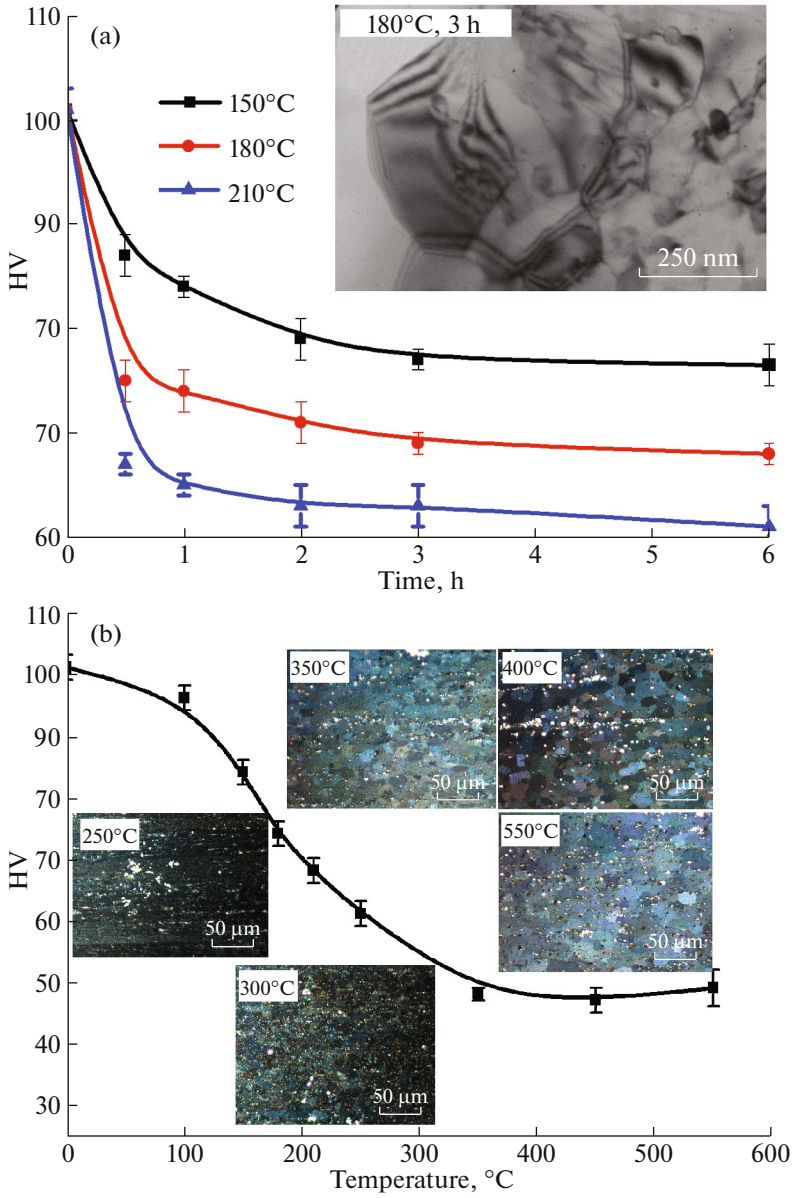

Fig. 4. Dependences of hardness of the rolled sheet on time after annealing at different temperatures (a) and on the annealing temperature for 1 h (b). Inset: (a) substructure by TEM, (b) grain structure by SEM.

Impurities of Fe and Si do not cause the formation of coarse lamellar intermetallic compounds and do not reduce the ductility of the alloy.

CONCLUSIONS

The effect of iron and silicon impurities (up to 0.15 wt %) on the phase composition and properties of Al–4.3Cu–2.2Yb quasi-binary alloy was studied. In addition to an aluminum solid solution and dispersed eutectic ((Al) + Al_8Cu_4Yb) in which about 1% Fe is dissolved, $Al_3Yb/(Al,Cu)_{17}Yb_2$ and (AlYbCuSi) phases with the approximate composition of $Al_{80}Yb_5Cu_6Si_8$ were found. After homogenization at 590°C for 3 h, the structure consists of compact fragmented and coagulated intermetallic compounds with a size of 1–2 μm and (Al) solid solution with the maximum copper content of 2.1%. Disordering in the rolled sheets during annealing at temperatures below 250°C is connected with recovery and polygonization processes; recrystallization occurs at $t > 300$°C. After annealing at 300°C for 1 h, the size of the recrystallized grain is 7 μm, and it grows to 16 μm at the annealing temperature of 550°C ($\tau = 1$ h). The conditional strength of the alloy with impurities is 205–273 MPa, and the tensile strength is 215–302 MPa at an elongation of 2.3–5.6% after annealing the rolled sheet. Fe and Si impurities do not cause the formation of coarse lamellar interme-

tallic compounds and do not reduce the ductility of the alloy.

FUNDING

This work was supported by the Russian Science Foundation (project no. 21-79-00193).

CONFLICT OF INTEREST

The authors declare that they have no conflict of interest.

REFERENCES

1. Zolotorevsky, V.S., Belov, N.A., and Glazoff, M.V., *Casting Aluminum Alloys,* New Kensington, PA: Alcoa Technical Center, 2007.
2. Belov, N.A. and Khvan, A.V., Structure and phase composition of alloys of the Al–Ce–Cu system in the region of the Al–Al_8CeCu_4 quasi-binary join, *Russ. J. Non-Ferrous Met.,* 2007, vol. 48, pp. 45–50.
3. Belov, N.A., Khvan, A.V., and Alabin, A.N., Microstructure and phase composition of Al–Ce–Cu alloys in the Al-rich corner, *Mater. Sci. Forum,* 2006, vols. 519–521, part 1, pp. 395–400.
4. Belov, N.A. and Khvan, A.V., The ternary Al–Ce–Cu phase diagram in the aluminum-rich corner, *Acta Mater.,* 2007, vol. 55, pp. 5473–5482.
5. Pozdniakov, A.V. and Barkov, R.Y., Microstructure and materials characterization of the novel Al–Cu–Y alloy, *Mater. Sci. Technol.,* 2018, vol. 34, no. 12, pp. 1489–1496.
6. Amer, S.M., Barkov, R.Yu., Yakovtseva, O.A., and Pozdniakov, A.V., Comparative analysis of structure and properties of quasi-binary Al–6.5Cu–2,3Y and Al–6Cu–4.05Er alloys, *Phys. Met. Metallogr.,* 2020, vol. 121, no. 5, pp. 476–482.
7. Pozdniakov, A.V., Barkov, R.Yu., Amer, S.M., Levchenko, V.S., Kotov, A.D., and Mikhaylovskaya, A.V., Microstructure, mechanical properties and superplasticity of the Al–Cu–Y–Zr alloy, *Mater. Sci. Eng., A,* 2019, vol. 758, pp. 28–35.
8. Amer, S.M., Barkov, R.Yu., and Pozdniakov, A.V., Effect of Mn on the phase composition and properties of Al–Cu–Y–Zr alloy, *Phys. Met. Metallogr.,* 2020, vol. 121, no. 12, pp. 1227–1232.
9. Amer, S.M., Barkov, R.Yu., Prosviryakov, A.S., and Pozdniakov, A.V., Structure and properties of new heat-resistant cast alloys based on the Al–Cu–Y and Al–Cu–Er systems, *Phys. Met. Metallogr.,* 2021, vol. 122, pp. 908–914.
10. Amer, S.M., Barkov, R.Yu., Prosviryakov, A.S., and Pozdniakov, A.V., Structure and properties of new wrought Al–Cu–Y and Al–Cu–Er based alloys, *Phys. Met. Metallogr.,* 2021, vol. 122, pp. 915–922.
11. Pozdnyakov, A.V., Barkov, R.Yu., Sarsenbaev, Zh., Amer, S.M., and Prosviryakov, A.S., Evolution of microstructure and mechanical properties of a new Al–Cu–Er wrought alloy, *Phys. Met. Metallogr.,* 2019, vol. 120, no. 6, pp. 614–619.
12. Amer, S.M., Barkov, R.Yu., Yakovtseva, O.A., Loginova, I.S., and Pozdniakov, A.V., Effect of Zr on microstructure and mechanical properties of the Al–Cu–Er alloy, *Mater. Sci. Technol.,* 2020, vol. 36, no. 4, pp. 453–459.
13. Amer, S.M., Mikhaylovskaya, A.V., Barkov, R.Yu., Kotov, A.D., Mochugovskiy, A.G., Yakovtseva, O.A., Glavatskikh, M.V., Loginova, I.S., Medvedeva, S.V., and Pozdniakov, A.V., Effect of homogenization treatment regime on microstructure, recrystallization behavior, mechanical properties, and superplasticity of Al–Cu–Er–Zr alloy, *JOM,* 2021, vol. 73, no. 10, pp. 3092–3101.
14. Amer, S., Yakovtseva, O., Loginova, I., Medvedeva, S., Prosviryakov, Al., Bazlov, A., Barkov, R., and Pozdniakov, A., The phase composition and mechanical properties of the novel precipitation-strengthening Al–Cu–Er–Mn-Zr alloy, *Appl. Sci.,* 2020, vol. 10, p. 5345.
15. Amer, S., Barkov, R., and Pozdniakov, A., Microstructure and mechanical properties of novel quasibinary Al–Cu–Yb and Al–Cu–Gd alloys, *Metals,* 2021, vol. 11, p. 476.
16. Amer, S.M., Barkov, R.Yu., and Pozdniakov, A.V., Effect of iron and silicon impurities on phase composition and mechanical properties of Al–6.3Cu–3.2Y alloy, *Phys. Met. Metallogr.,* 2020, vol. 121, no. 10, pp. 1002–1007.
17. Amer, S.M., Barkov, R.Yu., and Pozdniakov, A.V., Effect of impurities on the phase composition and properties of a wrought Al–6% Cu–4.05% Er alloy, *Phys. Met. Metallogr.,* 2020, vol. 121, no. 5, pp. 495–499.
18. Barkov, M.V., Mamzurina, O.I., Glavatskikh, M.V., Barkov, R.Yu., and Pozdnyakov, A.V., Influence of impurities on phase composition and properties of Al–Cu–Gd alloy, *Fiz. Met. Metalloved.,* 2022, vol. 123, no. 6, pp. 1–6.
19. Vo, N.Q., Dunand, D.C., and Seidman, D.N., Improving aging and creep resistance in a dilute A-Sc alloy by microalloying with Si, Zr and Er, *Acta Mater.,* 2014, vol. 63, pp. 73–85.
20. De Luca, A., Dunand, D.C., and Seidman, D.N., Mechanical properties and optimization of the aging of a dilute Al–Sc–Er–Zr–Si alloy with a high Zr/Sc ratio, *Acta Mater.,* 2016, vol. 119, pp. 35–42.
21. Booth-Morrison, C., Seidman, D.N., and Dunand, D.C., Effect of Er additions on ambient and high-temperature strength of precipitation-strengthened Al–Zr–Sc–Si alloys, *Acta Mater.,* 2012, vol. 60, pp. 3643–3654.
22. Pozdniakov, A.V., Aitmagambetov, A.A., Makhov, S.V., and Napalkov, V.I., Effect of impurities of Fe and Si on the structure and strengthening upon annealing of the Al–0.2% Zr–0.1% Sc alloys with and without Y additive, *Phys. Met. Metallogr.,* 2017, vol. 118, no. 5, pp. 479–484.
23. Pozdnyakov, A.V. and Barkov, R.Yu., Effect of impurities on the phase composition and properties of a new alloy of the Al–Y–Er–Zr–Sc system, *Metallurgist,* 2019, vol. 63, nos. 1–2, pp. 79–86.
24. Wen, S.P., Gao, K.Y., Huang, H., Wang, W., and Nie, Z.R., Role of Yb and Si on the precipitation

hardening and recrystallization of dilute Al–Zr alloys, *J. Alloys Compd.,* 2014, vol. 599, pp. 65–70.

25. Peng, G., Chen, K., Fang, H., and Chen, S., A study of nanoscale $Al_3(Zr,Yb)$ dispersoids structure and thermal stability in Al–Zr–Yb alloy, *Mater. Sci. Eng., A,* 2012, vol. 535, pp. 311–315.
26. Barkov, R.Y., Yakovtseva, O.A., Mamzurina, O.I., Loginova, I.S., Medvedeva, S.V., Proviryakov, A.S., Mikhaylovskaya, A.V., and Pozdniakov, A.V., Effect of Yb on the structure and properties of an electroconductive Al–Y–Sc alloy, *Phys. Met. Metallogr.,* 2020, vol. 121, no. 6, pp. 604–609.
27. Nhon, Q.Vo., Davaadorj, B., Amirreza, S., Evander, R., and Dunand, D.C., Effect of Yb microadditions on creep resistance of a dilute Al–Er–Sc–Zr alloy, *Materialia,* 2018, vol. 4, pp. 65–69.
28. Van Dalen, M.E., Gyger, T., Dunand, D.C., and Seidman, D.N., Effects of Yb and Zr microalloying additions on the microstructure and mechanical properties of dilute Al–Sc alloys, *Acta Mater.,* 2011, vol. 59, pp. 7615–7626.
29. Fang, H.C., Shang, P.J., Huang, L.P., Chen, K.H., Liu, G., and Xiong, X., Precipitates and precipitation behavior in Al–Zr–Yb–Cr alloys, *Mater. Lett.,* 2012, vol. 75, pp. 192–195.
30. Zhang, Y., Zhou, W., Gao, H., Han, Y., Wang, K., Wang, J., Sun, B., Gu, S., and You, W., Precipitation evolution of A–Zr–Yb alloys during isochronal aging, *Scr. Mater.,* 2013, vol. 69, pp. 477–480.
31. Fang, H.C., Chen, K.H., Chen, X., Chao, H., and Peng, G.S., Effect of Cr, Yb and Zr additions on localized corrosion of Al-Zn-Mg-Cu alloy, *Corros. Sci.,* 2009, vol. 51, pp. 2872–2877.
32. Chen, K.H., Fang, H.C., Zhang, Z., Chena, X., and Liu, G., Effect of Yb, Cr and Zr additions on recrystallization and corrosion resistance of Al–Zn–Mg–Cu alloys, *Mater. Sci. Eng., A,* 2008, vol. 497, pp. 426–431.
33. Song, M., Wu, Z., and He, Y., Effects of Yb on the mechanical properties and microstructures of an Al–Mg alloy, *Mater. Sci. Eng., A,* 2008, vol. 497, pp. 519–523.
34. Pozdnyakov, A.V., Barkov, R.Yu., and Levchenko, V.S., Influence of Yb on the phase composition and mechanical properties of low-scandium Al–Mg–Mn–Zr–Sc and Al–Mg–Cr–Zr–Sc alloys, *Phys. Met. Metallogr.,* 2020, vol. 121, no. 1, pp. 84–88.
35. Zolotorevskiy, V.S. and Pozdniakov, A.V., Determining the hot cracking index of Al-Si-Cu-Mg casting alloys calculated using the effective solidification range, *Int. J. Cast Met. Res.,* 2014, vol. 27, no. 4, pp. 193–198.
36. Zolotorevskii, V.S., Pozdnyakov, A.V., and Churyumov, A.Y., Search for promising compositions for developing new multiphase casting alloys based on Al–Zn–Mg matrix using thermodynamic calculations and mathematic simulation, *Phys. Met. Metallogr.,* 2014, vol. 115, no. 3, pp. 286–294.
37. Shurkin, P.K., Belov, N.A., Musin, A.F., and Aksenov, A.A., New high-strength casting Al–Zn–Mg–Ca–Fe-based aluminum alloy without heat treatment, *Russ. J. Non-Ferrous Met.,* 2020, vol. 61, no. 2, pp. 179–187.
38. Shurkin, P.K., Belov, N.A., Musin, A.F., and Samoshina, M.E., Effect of calcium and silicon on the character of solidification and strengthening of the Al–8% Zn–3% Mg alloy, *Phys. Met. Metallogr.,* 2020, vol. 121, no. 2, pp. 135–142.
39. Belov, N.A., Naumova, E.A., Doroshenko, V.V., and Avxentieva, N.N., Combined effect of calcium and silicon on the phase composition and structure of Al–10% Mg alloy, *Russ. J. Non-Ferrous Met.,* 2018, vol. 59, pp. 67–75.
40. Loginova, I.S., Sazera, M.V., Popov, N.A., Pozdnyakov, A.V., and Solonin, A.N., Features of structure formation in an Al–Fe–Mn alloy upon crystallization with various cooling rates, *Russ. J. Non-Ferrous Met.,* 2021, vol. 62, pp. 72–81.
41. Belov, N.A., Naumova, E.A., Doroshenko, V.V., and Bazlova, T.A., Effect of scandium on the phase composition and hardening of casting aluminum alloys of the Al–Ca–Si system, *Russ. J. Non-Ferrous Met.,* 2016, vol. 57, pp. 695–702.
42. Belov, N.A., Alabin, A.N., Sannikov, A.V., and Deev, V.B., Primary crystallization in the Al–Fe–Mn–Ni–Si system as applied to casting alloys based on aluminum-nickel eutectic, *Russ. J. Non-Ferrous Met.,* 2014, vol. 55, pp. 356–364.
43. Huang, G., Liu, L., Zhang, L., and Jin, Z., Thermodynamic description of the Al–Cu–Yb ternary system supported by first-principles calculations, *J. Min. Metall., Sect. B.,* 2016, vol. 52, pp. 177–183.

Translated by N. Saetova